Sensors and Actuators A 157 (2010) 328–335

Contents lists available at ScienceDirect

Sensors and Actuators A: Physical

journal homepage: www.elsevier.com/locate/sna

Dissipative particle dynamics simulation of entropic trapping for DNA separation

H. Pan, T.Y. Ng*, Hua Li, E. Moeendarbary

School of Mechanical & Aerospace Engineering, Nanyang Technological University 50 Nanyang Avenue, Singapore 639798, Singapore

ARTICLE INFO

Article history:
Received 23 June 2009
Received in revised form
16 November 2009
Accepted 25 November 2009
Available online 3 December 2009

Keywords:
Entropic trapping device
DNA separation
Multiphase and particle-laden flow
Dissipative particle dynamics

ABSTRACT

The dissipative particle dynamic (DPD) method is applied to simulate the DNA separation process based on a mechanism developed earlier by other authors, who demonstrated a micro-device for separating DNA molecules (>2 kbp) through an entropic trapping mechanism. The DPD is used to model the process because it is intrinsic to modeling hydrodynamic interactions, which is lacking in some earlier works. We use the worm-like chain model to represent DNA molecule and Lennard–Jones potential at mesoscopic level to avoid phantom collision between the chain beads. Our simulations show that longer DNA strands do move faster than shorter ones, as observed in available experimental data. We also confirm that the delayed entrance is the cause of entropic trapping. Contrary to some earlier reported data, we found that the corner trapping is not a contributor to DNA separation.

1. Introduction

DNA separation is important for various biological analyses, such as DNA fingerprinting and genome sequencing. Gel electrophoresis is the standard method for separation DNA by length. However, it is efficient only for DNA molecules up to 40 kbp (base pairs). Slab gel pulsed-field gel electrophoresis (PFGE) can be used to separate longer double-stranded DNA (dsDNA), but the process usually takes several days if not weeks. Many researchers have proposed novel separation mechanisms using on micro- and/or nano-fluidic devices [1–4]. Turner et al. [5] presented a device capable of separating DNA molecules according to their length. This device consists of pillar-free and pillared regions. A dense matrix of nanopillars with a diameter of 35 nm and spacing of 160 nm is fabricated in the pillared region. When the driving electric field is applied, DNA molecules are forced into the pillared region where they are stretched to fit nano-channels inside the pillar matrix. When the entire small molecule enters the pillar matrix and only part of large molecule enters, the electric field is turned off. The large molecule will recoil back in the pillar-free region because of the tendency to maximize its conformational entropy and the small molecule will stay inside the matrix due to uniform entropy. Therefore, the molecules of different lengths can be separated. Bakajin et al. [6] manufactured a micro-chamber with hexagonal array of pillars 2 μm wide where transverse pulsed electrical fields are applied alternatively along two axes of the array, separated by 120°. Shorter molecules move faster in the array because they spend less time to reorient themselves along the axis of the field, while longer molecules use most of the pulse period to entirely align to the axis of the field. Huang et al. [7] applied a similar idea to fabricate a DNA prism where DNAs of different sizes are force to follow different route inside the micro-structured sieving matrix under the asymmetric pulsed electric field. Han et al. [1–3] developed an entropic trapping array, which consists of alternative deep and shallow channels, to separate long DNA molecules (>2 kbp). The shallow section is smaller than molecule at maximum entropy state so that the molecules must be stretched to pass through. Size-dependent trapping is produced because entropic free energies for DNA molecules of different sizes are different in the deep and shallow sections. Thus, the separation is enabled using a micro-fabricated entropic trapping array. More recently, Fu et al. [8] followed Han et al.'s [1,2] work and introduced an anisotropic nanofilter array (ANA) for continuous-flow biomolecule separation, where both small molecules and long molecules can be separated through Ogston sieving and entropic trapping mechanism respectively. Fu et al. [9] also demonstrated the separation of proteins with different charges in ANA.

Besides the experimental studies mentioned above, numerical simulation provides an alternative route to study DNA separation process. Micro-channels used in the DNA separation have characteristic size between dozens of nanometers and several micrometers and length around several millimeters. Because of the molecular scales involved, direct simulation, such as molecular dynamics (MD), is very expensive, if not completely infeasible. Furthermore, DNA mechanical properties at mesoscopic scale (0.1 μm) levels are physically relevant for understanding the separation process. Various mesoscopic methods have been applied in this area. Tessier et al. [10] performed Monte Carlo simulation of DNA flow

* Corresponding author.
E-mail address: mtyng@ntu.edu.sg (T.Y. Ng).

0924-4247/$ – see front matter © 2009 Elsevier B.V. All rights reserved.
doi:10.1016/j.sna.2009.11.027

through entropic trap array where polymer is modeled by a lattice model with bond fluctuation. Their results confirmed Han et al.'s [1,2] finding that longer molecules were trapped for shorter times. However, the trapping time was unexpectedly long in their simulation and this could be due to the discrete lattice chain model. Streek et al. [4] employed the Brownian dynamics (BD) method to simulate the same process and they used the chain model with linear spring to represent the DNA. However, they did not include the hydrodynamics interaction (HI) in their BD model. They found two mechanisms contributing to longer trapping times for smaller molecules, namely delayed entrance of the narrow channel and trapping at the corner of the channel. They also claimed that the second mechanism, which is due to recirculation flow near the corner, is the dominating factor. On the other hand, Lee [11] found through experiments that shorter DNA can move faster than longer ones in similar alternating deep–shallow nano-channels. We venture to postulate that the second trapping mechanism (corner trapping) may not be valid since the gradient of the electric potential smoothly converges to the entrance of the narrow region and the charged molecules, such as DNA, should follow the electric field in the electrophoresis process despite the thermo-fluctuation. As will be presented later in this paper, we found no corner trapping mechanism in our simulation. The lack of hydrodynamic interaction may contribute this converse deduction in Streek et al.'s [4] BD simulation. Perkins et al. [12] claimed that "DNA is not free-draining even near full extension". According to Viovy [13], the hydrodynamic interaction is not negligible for DNA undergoing electrophoresis. Jendrejack et al. [14] also claimed that the hydrodynamic interaction model provides results which quantitatively agree with experimental data. Therefore, we strongly believe that correctly modeling the hydrodynamic interaction is very important for the simulation of DNA undergoing electrophoresis.

Instead of BD, a different mesoscopic method, namely the dissipative particle dynamics (DPD) is employed in this work. The DPD method (Hoogerbrugge and Koelman [15] and Español and Warren [16]) is a particle-based method which is able to effectively capture the dynamical and rheological properties at length scales orders of magnitude larger than molecular scales. Each particle represents "a collection of molecules" and interactions between them are represented through soft repulsion, dissipation and stochastic noise. Compared to BD, the DPD has an advantage in that the hydrodynamic interaction is intrinsic. The DPD is extremely versatile for the construction of simple models for complex fluids, as indicated in Español [17]. It has been applied in various applications, including hydrodynamics of Newtonian fluid (Español and Warren [16]), colloidal suspension (Boek et al. [18]), polymer solution (Kong et al. [19] and Fan et al. [20]), multiphase flow (Conveney and Novik [21] and Liu et al. [22]), etc. In this paper, we study DNA separation in micro-channels using the DPD method.

To model macromolecules, such as polymer and DNA, in mesoscopic simulations, various coarse-graining models have been developed, including the freely jointed chain (FJC), freely rotating chain (FRC) and rotational isometric state (RIS) chain. In FJC, each bond is treated as a free joint and the bond itself is modeled as a rod or spring. The FRC is similar to FJC except that the angles between bonds are fixed. The RIS is more complicated and includes rotation between bonds. Although the RIS has been more successful in determining the equilibrium properties of polymers, coarser models, such as the FJC are sufficient for understanding the dynamics of long chain molecules according to UnderHill and Doyle [23]. After coarse-graining, a chain macromolecule is represented as a series of beads connected by either rods or springs. Rigid constraints exist in bead-rod chains while elastic restoring forces are applied in bead-spring chain models. The restoring forces are primarily due to the entropy of the molecules. The entropy is mostly measured by the number of micro-states, which are at small scale and are neglected in coarse-graining. A variety of numerical models have been developed to represent these entropic restoring forces, including the Hookean spring, the inverse Langevin function spring, the finitely extensible non-linear elastic (FENE) spring and the worm-like chain (WLC). These numerical chain models are used to model polymer and DNA molecules in various applications. In particular, the WLC model is well suited for describing stiff polymers and is effectively used to model DNA molecules. Smith et al. [24,25] used real-time fluorescence microscopy to directly measure the extension of single DNA under different forces and created the extension versus force curves for individual DNA molecules, which was used by Bustamante [26] to construct parameters for the WLC model. Perkins et al. [12] measured the extension of the DNA molecule in flow using optical tweezers and fluorescence microscopy and found quantitative agreement between elasticity data and the WLC force law. They also claimed that the hydrodynamic interaction between solvent and DNA is not negligible during electrophoresis. Marko and Sigga [27] analyzed the experiments presented by Smith et al. [24], Schurr and Smith [28] and Perkins et al. [12] and found clear signature of WLC elasticity in the force-extension relations.

In this paper, we use DPD to simulate DNA separation process through entropic trapping mechanism. Sections 2 and 3 respectively present the DPD method and the coarse-grain DNA model. Wall boundary treatment, integration algorithm and parallelization are briefly described in Sections 4–6 respectively. Scaling of radius of gyration of DNA model is presented in Section 7 to validate the DNA model. The DNA separation simulation results are presented and discussed in Section 8. Finally, the conclusions are drawn.

2. The dissipative particle dynamics (DPD) method

In the DPD method, the system consists of interacting point particles, which are a representation of a group of real molecules. The motions of these point particles are governed by Newton's equations of motion. The forces between these point particles are assumed to be pairwise additive. For the ith particle, we have the governing equations:

$$\frac{d\vec{r}_i}{dt} = \vec{v}_i \tag{1}$$

$$\frac{d\vec{v}_i}{dt} = \sum_{i \neq j} \vec{f}_{ij} + \vec{f}_i^{ext} \tag{2}$$

Here $\vec{r}_i$ and $\vec{v}_i$ denote the position and velocity vectors respectively. The subscripts i and j represent the particle index. We assume all particles have identical mass, which is taken as the unit of mass. $\vec{f}_{ij}$ is the DPD inter-particle force acting from the jth particle to the ith particle. $\vec{f}_i^{ext}$ is the external force, such as the electric force in electrophoresis, acting on the ith particle.

In DPD, a particle represents a group of molecules and the interaction between particles can be loosely interpreted as a collective representation of forces between these two groups of molecules. The inter-particle force consists of three parts, namely: a conservative force $\vec{f}_{ij}^C$, a dissipative force $\vec{f}_{ij}^D$ and a stochastic force $\vec{f}_{ij}^R$:

$$\vec{f}_{ij} = \vec{f}_{ij}^C + \vec{f}_{ij}^D + \vec{f}_{ij}^R \tag{3}$$

The conservative force $\vec{f}_{ij}^C$ is a soft repulsion force acting along the line of particle centers and is given by:

$$\vec{f}_{ij}^C = \vec{f}^C(\vec{r}_{ij}) = \begin{cases} a_{ij}(1 - r_{ij}/r_c)\vec{e}_{ij}, & r_{ij} \leq r_c \\ 0 & r_{ij} > r_c \end{cases} \tag{4}$$

where a_{ij} is the maximum repulsion. $\vec{r}_{ij} = \vec{r}_i - \vec{r}_j$ is the vector from the jth particle to the ith particle and $\vec{e}_{ij} = \vec{r}_{ij}/\left|\vec{r}_{ij}\right|$ gives its unit vec-

tor direction, and r_c is the cutoff radius. The conservative force is a linear function of particle distance. The dissipative force acts as viscous force in the system to reduce velocity difference between particles. The stochastic force represents the thermal motion of unresolved scales, such as the molecules inside each particle. The dissipative and stochastic forces are given by:

$$\vec{f}_{ij}^{D} = \vec{f}^{D}(\vec{r}_{ij}) = -\gamma w^{D}(r_{ij})(\vec{e}_{ij}\cdot\vec{v}_{ij})\vec{e}_{ij} \tag{5}$$

$$\vec{f}_{ij}^{R} = \vec{f}^{R}(\vec{r}_{ij}) = \sigma w^{R}(r_{ij})\theta_{ij}\vec{e}_{ij} \tag{6}$$

Here γ and σ are two coefficients that control the strengths of the dissipation and random forces. $w^D(r_{ij})$ and $w^R(r_{ij})$ are weight functions, and are dependent on the particle distance. $\vec{v}_{ij} = \vec{v}_i - \vec{v}_j$ and θ_{ij} is a white noise function with the following properties:

$$\langle\theta_{ij}(t)\rangle = 0,\ \theta_{ij}(t)\langle\theta_{ij}(t)\theta_{kl}(t')\rangle = (\delta_{ik}\delta_{jl} + \delta_{il}\delta_{jk})\,\delta(t-t') \text{ with } i\neq j \text{ and } k\neq l \tag{7}$$

The stochastic force acts to "heat up" the system. The dissipative force, on the other hand, removes the kinetic energy and cools down the system. When a balance is reached, the system's temperature will remain constant. According to the fluctuation–dissipation theorem as stated in Español and Warren [16], the following relations must hold in order to guarantee the system reaches equilibrium at the specific temperature T:

$$w^{D}(r) = [w^{R}(r)]^2 \text{ and } \sigma^2 = 2\gamma k_B T \tag{8}$$

Here k_B is the Boltzmann constant. A widely adopted weight function is

$$w^{D}(r) = [w^{R}(r)]^2 = \begin{cases} (1-r/r_c)^2, & r \le r_c \\ 0, & r > r_c \end{cases} \tag{9}$$

Furthermore, Fan et al. [20] proposed a general weight function to improve the Schmidt number of DPD system:

$$w^{D}(r) = [w^{R}(r)]^2 = \begin{cases} (1-r/r_d)^s, & r \le r_d \\ 0, & r > r_d \end{cases} \tag{10}$$

Here r_d is cut-off distance for diffusive and stochastic forces. It may be different from r_c, which is the cut-off distance used when calculating the soft repulsion force. Fan et al. [20] systematically studied the effects of the parameters s and r_d on diffusivity, viscosity and Schmidt number and used $s = 0.5$ in their simulations. The choice of r_d affects the number of pairs of interacting particles and the computation cost. In this paper, we adopt $r_d = r_c = 1$.

3. The DNA model

Large DNA molecules are represented as a series of particles (beads) linked through springs. Various numerical models have been constructed, such as the Hookean and FENE models. The mechanical properties of a single DNA molecule have been extensively studied experimentally. Marko and Sigga [27] analyzed the experiments presented by Smith et al. [24] and Schurr and Smith [28]. Perkins et al. [12] found the mechanical properties of DNA molecule in an aqueous solution can be realistically modeled using the worm-like chain (WLC) model, where the attraction spring force between successive beads is expressed as

$$f_{i,i+1}^{WLC} = -\frac{k_B T}{4\lambda_p^{eff}}\left[\left(1-\frac{r_{i,i+1}}{l}\right)^{-2} + 4\frac{r_{i,i+1}}{l} - 1\right] \tag{11}$$

where λ_p^{eff} is the effective persistence length and l the length of fully extended spring. The contour length of a DNA molecule $L = l(N_b - 1)$ where N_b is the number of beads and $N_b - 1$ the number of springs.

UnderHill and Doyle [23] used statistical mechanics to analyze the bead-spring chain models. They provided a bound on the number of beads used to model the molecule, $15 \le N_b \le 0.01\alpha$, where α is the number of persistence length segments that molecule contains. They also provided the choice of correction factor of the effective persistence length. Various physical problems of a single DNA, such as scaling of radius of gyration and extension under force/shear, have been successfully studied using the WLC model.

In this paper, we use standard DPD particles to represent the chain beads, and the DNA molecule is modeled as a string of DPD particles which is sequentially connected through the WLC spring. However, the DPD particles can pass through each other without restriction. It was observed that the chain beads pass through each other during the simulation and caused the problem of phantom collisions. In order to enforce self-avoidance of the chain, we apply the Lennard–Jones potential U^{LJ} between beads as in Symeonidis et al. [29]. It is noted that the Lennard–Jones potential applied here is defined at mesoscopic level and not at the microscopic level as in molecular dynamics. When the beads get close, the repulsion force derived from the Lennard–Jones potential will dominate and push them apart. The repulsion force is calculated as follows:

$$f^{LJ}(r_{ij}) = -\nabla U^{LJ} = \frac{24\varepsilon}{r_{ij}}\left(\frac{\sigma_{LJ}}{r_{ij}}\right)^6\left[2\left(\frac{\sigma_{LJ}}{r_{ij}}\right)^6 - 1\right] \tag{12}$$

where ε is the depth of the potential well and σ_{LJ} is the distance at which the potential equals to zero.

In summary, the DNA molecule is modeled as a string of beads linked by springs. The spring force between successive beads is specified by Eq. (11) while the inter-bead repulsion force given by Eq. (12) is used to ensure self-avoidance.

4. The wall boundary

In the simulation of complex flows, one has to consider the solid wall boundary. There are various ways to model wall boundary in DPD. In the Lee–Edwards boundary condition as shown in Lee and Edwards [30], periodic images outside the simulation box are applied to ensure the desired shear rates. Many researchers, such as Revenga et al. [31] and Willemsen et al. [32], also used frozen particles to represent the solid surface, which interact with other particles. Due to the soft repulsion between particles, it is difficult to prevent particles from penetrating the wall boundary. Furthermore, large density fluctuation is also observed near wall boundary in this kind of wall treatment. Several methods have been developed to remedy these problems. Besides higher density of wall particles, particle reflection schemes have also been adopted to shift particles, which ventured inside the wall, back into the fluid domain, so as to maintain mass conservation and prevent wall penetration. Revenga et al. [33] carried out a detailed study on various reflection methods, including specular, Maxwellian and bounce back reflections. Willemsen et al. [32] presented a method to reduce density fluctuation near wall boundary. They created an extra layer of "ghost" particles within the interacting distance from the wall and computed their positions and velocities using the positions and velocities of particles inside the simulation domain. Although their method is complex and expensive, it significantly reduced the density fluctuation near the wall boundary. Duc et al. [34] used two layers of wall particles to provide smooth repulsion against the fluid particles and bounce-back reflection to correct particle penetration. Their calculations showed reduction in the density fluctuation near the wall boundary, and the no-slip boundary was also well-preserved.

In this paper, we adopt Duc et al.'s [34] method because of its simplicity, and the use of only local operations. We generate two layers of wall particles along the wall boundary. The distances from

the first and second layer wall particles to the boundary are $\alpha_1 r_c$ and $\alpha_2 r_c$ respectively, where $0 < \alpha_1 < \alpha_2 < 1$. These wall particles interact with free particles in the same way as the interaction between free particles themselves. To prevent penetration, the bounce back reflection is applied to particles inside the wall boundary. The new position and velocity of the particle after bounce back reflection are given as follow

$$\vec{v}_{new} = 2\vec{v}_{wall} - \vec{v}_{old}$$
$$\vec{r}_{new} = \vec{r}_{old} + 2d_n\vec{n}_{wall} \quad (13)$$

where d_n is the distance between the particle and wall boundary, and $\vec{n}_{wall}$ is the unit normal vector of the wall boundary. More details of the implementation of the wall boundary can be found in Duc et al. [34]. In our simulations, we choose $\alpha_1 = 0.125$ and $\alpha_2 = 0.125$.

5. Integration algorithm

Several integration schemes can be used for evolving the DPD governing equation. Lowe [35] presented a scheme based on the re-equilibration of the system where the dissipative and random forces are not explicitly calculated. The particle velocity is corrected at every time-step using the Maxwell velocity distribution. Groot and Warren [36] described a velocity-Verlet algorithm which is based on a prediction and correction procedure. The interaction forces are explicitly calculated. Both methods introduce minor artifacts as demonstrated in Jakobsen et al. [37]. The velocity-Verlet algorithm is popular because it is explicit and easier to be parallelized. It has been noted that the Lennard–Jones potential is a hard potential and increases exponentially with decreasing of distance. To ensure the stability of numerical integration, one can either use special integration schemes, such as sub-cycling as in Symeonidis and Karniadakis [38], or employ small time-steps. In this paper, we apply the standard velocity-Verlet algorithm with small time-step to avoid complexity and uncertainty of numerical errors introduced in sub-cycling.

6. Parallel implementation

With the exception of force calculations, all operations in the velocity-Verlet algorithm are local and can be easily parallelized. In the force calculations, the information of two particles within the cut-off distance are required, as shown in Eqs. (4)–(6). To reduce computation cost, Rapaport [39] presented a cell subdivision method. He divided the domain into sets of small Cartesian cells that have spans larger than the cut-off distance. Therefore, all interacting particle pairs must locate either in the same or neighboring cells. Instead of calculating the distance between any two particles, one only needs to test particles in same cell or neighboring cells. Using the linked-list data structure, it is a very efficient technique for identifying all interacting particle pairs.

To parallelize the force calculations, one must divide the particles among processors. In our implementation, we apply a domain decomposition technique. Cartesian cells are divided between processors and each processor holds all particles inside its cell partition. To further reduce the communication cost, the particles belonging to neighboring cells are duplicated and kept in the processor. Thus, the interacting particle pairs can be easily found. The partition strategy is to distribute cells among the processors so that each processor has nearly the same number of particles. Processors exchange only particle data belonging to neighboring cells. By doing so, we obtain better scalability, which is demonstrated in the following section. The code uses MPI to communicate data in different processors.

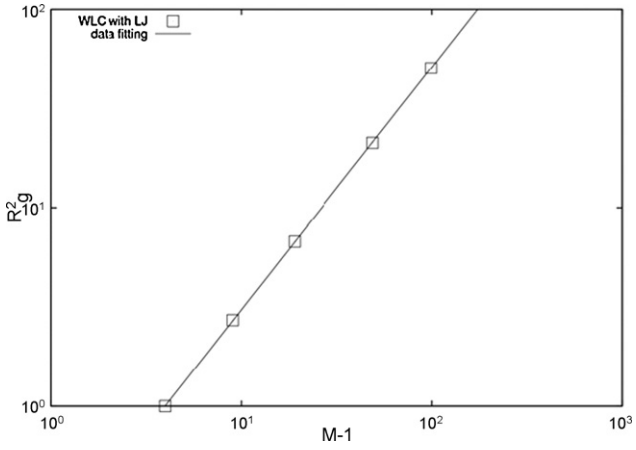

Fig. 1. Scaling of radius of gyration of DNA model using WLC and Lennard–Jones potential.

7. Scaling of radius of gyration

To verify the DNA model used in this work, we studied the scaling of radius of gyration of our chain model consisting of WLC and Lennard–Jones potential. The elastic property of the chain model, such as extension under force and/or shear, is another check for applicability of the chain model. For a chain under extension, the inter-bead force caused by the Lennard–Jones potential is negligible since it is active only when the beads are too close. We expect our chain model to possess similar properties as a pure WLC model, and the simulation results do indeed confirm this. The extension of WLC chains was comprehensively studied by Bustanmante [26] and Marko and Sigga [27] and we do not repeat it here.

Symeonidis et al. [29] studied the scaling of the radius of gyration of a single polymer using different chain models, including FENE, FENE with Lennard–Jones, and WLC. However, the scaling for WLC with Lennard–Jones, which is the DNA model used in this work, was not covered in that work. To verify this DNA model, we study the scaling of radius of gyration of a single DNA molecule. The radius of gyration of a chain is computed as follow

$$R_g^2 = \left\langle \frac{1}{N_b}\sum_{i=1}^{N_b}(\vec{r}_i - \vec{r}_{cm})^2 \right\rangle \quad (14)$$

where $\vec{r}_{cm} = \frac{1}{N_b}\sum_{i=1}^{N_b}\vec{r}_i$ is the position vector of center of mass. Statistical scaling arguments show that $R_g \propto (N_b - 1)^a$. For real chains, Flory's formulae gives $a = 0.6$, which has been verified by light scattering experiments reported in Gennes [40].

A single chain of multiple beads representing a DNA molecule is immersed in a box of DPD particles which models the solvent. Periodic boundaries are assumed on all six boundaries. Initially, the beads' positions are randomly generated. We allow the system to evolve until it reaches quasi-steady state, i.e. the highest entropy state. The DPD parameters used in Groot and Warren [36] are used in these simulations, where $\rho = 4, k_BT = 1, a_{ij} = 18.75$ and $\sigma = 3$. The same DNA model parameters as in Symeonidis et al. [29] are used here. We take $l = 2r_c$ and adjust the effective persistence length λ_p^{eff} using the results of UnderHill and Doyle [23] for λ-phage DNA. For the Lennard–Jones potential, $\varepsilon = k_BT$ and $\sigma_{LJ} = 2^{-1/6}$, so that only pure repulsion force acts between beads.

Simulations were carried out for chains with 5-, 10-, 20-, 50- and 100-beads. We measured the chains' radius of gyration in the simulations, and used the average as their radius of gyration. Fig. 1 presents the radius of gyration of chains of different length in logarithmic scale. The horizontal-axis is the number of springs and the

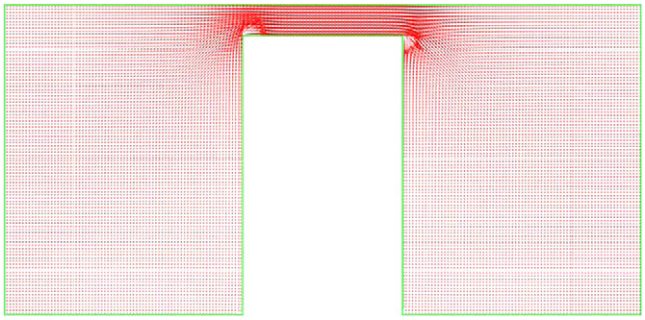

Fig. 2. Electric fluxes at the deep and shallow channels.

vertical-axis the radius of gyration. To calculate the scaling exponent, we fitted the result using non-linear least-squares theory and plotted it as the solid line in the figure. The static exponent of the scaling of radius of gyration for our DNA model is 0.609, which is close to the Flory's formulae.

8. DNA separation process

Han et al. [1,2] described a micro-channel device to separate DNA molecules of different sizes. This device consists of an array of micro-fabricated alternating deep and shallow regions. The deep channel is large enough to allow molecule relaxation to reach the maximum entropy state. The shallow channel is of nanometer scale, and is smaller than the radius of gyration of the molecules. Therefore, the molecules have to deform before they pass through the shallow section. Conformation change from the maximum entropy state means that energy is required to match increasing entropic free energy. Han et al. [1,2] used a static electric field to drive the DNA molecules. Fig. 2 presents a period of Han et al.'s [1,2] micro-channel and the electric field inside it. The green lines represent the boundary of computational domain. The left and right boundaries are periodic boundaries and the particles that move out from either side are reintroduced at another side. The top and bottom boundaries are the channel wall boundaries. We neglect the solvent ions and surface charges on the channel wall when we solve the Laplacian equation for the electric potential. The vectors in the figure represent the reversed electric fluxes. The fluxes in the shallow channel are larger than in deep channel and their ratio is inversely proportional to the depth ratio. It is also noted that strong converging fluxes exist near the entrance and exit of the shallow channel. Fig. 3 highlights the strong converging and diverging fluxes, respectively.

The competition between entropic elasticity and electric driving force determines if molecules are able to squeeze into the shallow channels. According to Han et al. [1], molecules would be trapped indefinitely if the electric field is too weak to overcome the energy barrier, or escape without being retarded if the electric field is too strong. For either case, no separation occurs. When an appropriate electric field is applied, the molecules have finite possibility to overcome the energy barrier. Long DNA molecules have better chance to escape the entropic trap because they are more likely to develop narrow extrusion inside the shallow channel where the electric force is strong and pulls the entire molecule into the shallow channel. Han and Craighead [3] presented theoretical analyses on these phenomena. In the present work, we numerically study this entropic trapping mechanism using DPD simulation.

In the present simulation, the channel geometry was modified in order to reduce computation cost. We reduced the periodic channel length from 4 to 2 μm since we found that the molecules relax within short distances in the deep region. Therefore, it is not necessary to use a long channel to allow the chain to relax. The lengths

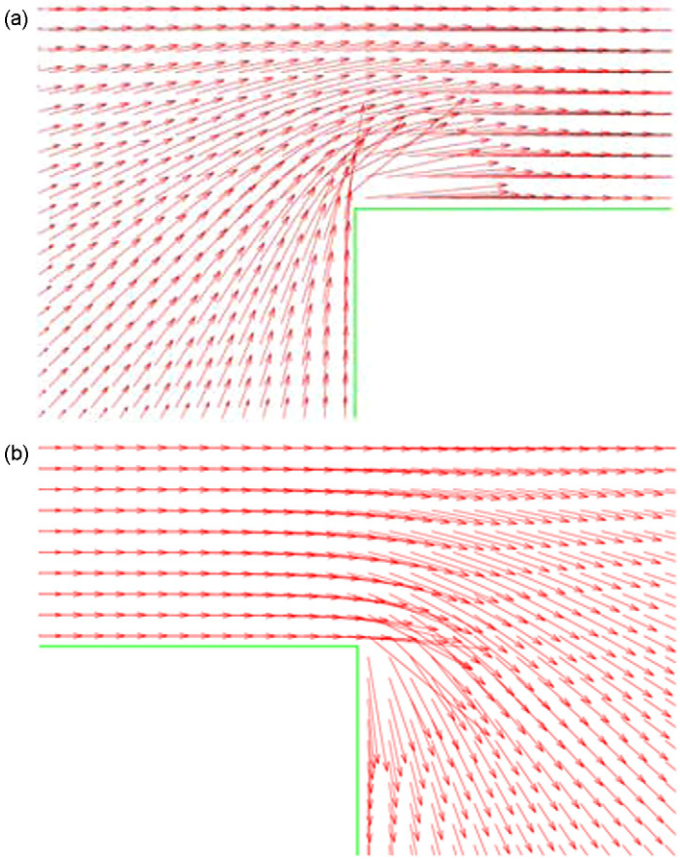

Fig. 3. Electric fluxes at entrance and exit of the shallow section.

of the shallow and deep regions are equal. The depth of the shallow region is set at 100 nm and the depth of deep region is reduced to 1 μm. In the actual experiment, the channel width is 30 μm. Here we use a width of 1 μm and apply periodic boundary condition in this direction. Two DNA models, one with 33 beads and the other with 129 beads, are considered here. The length ratio between these two models is close to the T2- and T7-DNA used in the experiment. We take the length scale as 50 nm and the shallow region has a non-dimensional depth of 2. In the current simulation, we use non-dimensionalized units, and the "2" here means that the depth is 100 nm since the length scale is 50 nm. We use the same parameters as indicated in the last section. The driving force acting on the particles is computed through interpolation of the electric flux field.

We conduct the simulations in the following manner. First, we generate chain models randomly inside the channel and allow relaxation without the influence of external force. Then, in order to mimic the accumulation stage of the experiment, we apply a small force so that the chain models accumulate at the front of shallow region. We found that the chains remained in the trap if the small external force is not increased, even when the simulation is run continuous for a very long time. This observation agrees with Han et al.'s [1,2] theory that the molecule would be trapped indefinitely when electric field is too weak. The last stage in the experiment is to launch the separation process by a sudden increase of the applied voltage. This process is simulated by increasing the electric fluxes to push the chain models such that they escape the trap.

Fig. 4 presents two simulation snapshots of the molecules' conformations during the separation process. In the deep channel, both molecules coil and relax to reach their maximum entropy states. Once they are in shallow channel, the molecules are stretched to fit into the limited space. Both molecules continuously alter their

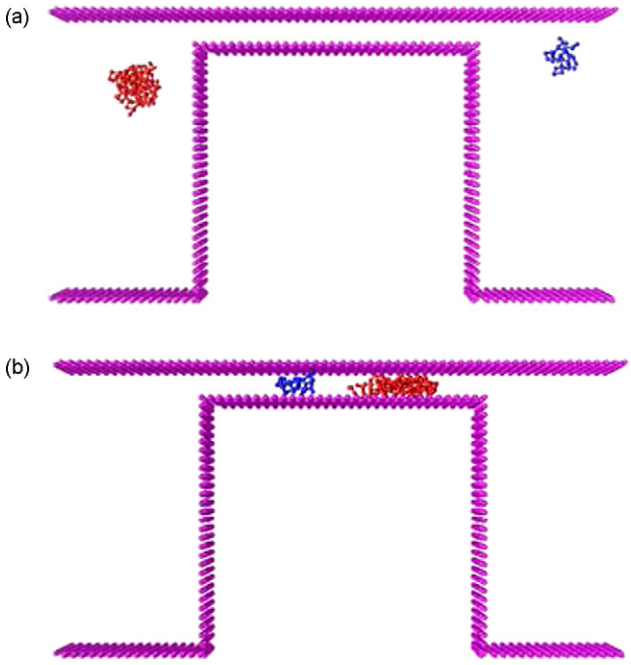

Fig. 4. The molecules' conformation change during electrophoresis.

conformations, between coil and stretch, during the electrophoresis.

Several simulations using different driving forces were conducted and separation of the chain models was observed. In this work, we define the chain position as the position of its center of mass. To directly measure the chain's movement, we use the chain's horizontal position and accumulate it over the periodic boundary. Fig. 5 shows the separation between short and long DNA models. Since our simulation is conducted on periodic domain, the movement of DNAs was accumulated horizontally to represent their movement passing through multiple traps. The figure presents the horizontal movement of the short and long chains under different driving forces. The horizontal-axis represents the simulation time while the vertical-axis represents the chain's accumulated horizontal position. Different magnitudes of the driving force are applied by multiplying different scalars to the interpolated electric fluxes. The figure shows the DPD simulation results using three scalars $f = 0.2, 0.4, 0.8$. In general, these curves indicate that molecules move faster when driving force is larger. Separation between short and long molecules is observed when $f = 0.2, 0.4$. For a weak force, $f = 0.2$, the velocity difference is large and the separation is efficient. However, the molecules move relatively slower and significant time is required for separation. When $f = 0.4$, the velocity difference is smaller compared to the case of $f = 0.2$. However, the molecules move faster. One can thus conclude that a small force results in clear separation but slow movement, while a larger force moves the chains faster but produces less efficient separation. When the driving force is too large, such as $f = 0.8$, both molecules move with similar velocities and no separation occurs. These observations agree with Han et al.'s [1,2] experimental findings. It should be noted out that we did not detect any corner trapping phenomenon as reported by Streek et al. [4] in our simulations. The electric fluxes converge to the entrance of shallow channel and always pull the molecules towards the entrance of shallow channel. No corner recirculation was observed in our simulations.

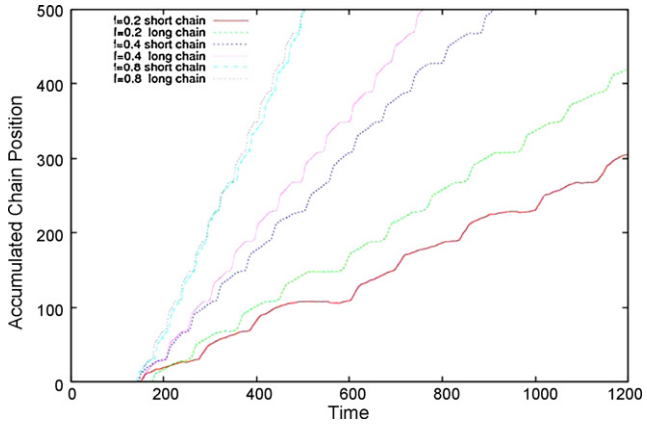

Fig. 5. Movements of short and long chains at different driving forces.

Table 1
Time scales for short and long chains.

Number of beads	τ_{app}	τ_{act}	τ_{cross}
33	1.34e2	1.83e1	1.19e1
129	7.83e1	1.18e1	1.45e1

Fig. 5 also shows that the molecule's horizontal motion is not linear. It actually contains three phases as indicated by Panwar and Kumar [41]. These three phases are namely: the approaching phase, where the molecule closes in at the entrance of the shallow channel; the activation phase, where the molecule changes its conformation to squeeze into the shallow channel; and the crossing phase, where the molecule passes through the narrow channel. Panwar and Kumar [41] conducted numeric studies using Brownian dynamics to identify the time scales associated with these three phases. We shall denote these time scales as τ_{app}, τ_{act} and τ_{cross}, respectively. They concluded that τ_{app} and τ_{act} decrease with molecule length while τ_{cross} increases with molecule length. We measured these time scales in our simulation where $f = 0.2$. The averaged time scales are presented in Table 1. Comparing the time scales for short and long chains, we find that our simulation results agree with Panwar and Kumar's [41] conclusions.

To verify our simulation results are time-step independent, we carried out corresponding simulations using four different time-steps, namely: 1e−3, 2e−3, 4e−3 and 8e−3. The driving force scalar is set to $f = 0.4$. Fig. 6 demonstrates the time-step convergence of simulations since time-step does affect the DPD simulation results. The figure presents horizontal movement of the short and long molecules using different integration time-steps. It is demonstrated that the time-step does affect the DPD simulations. The molecules move with different trajectories when different

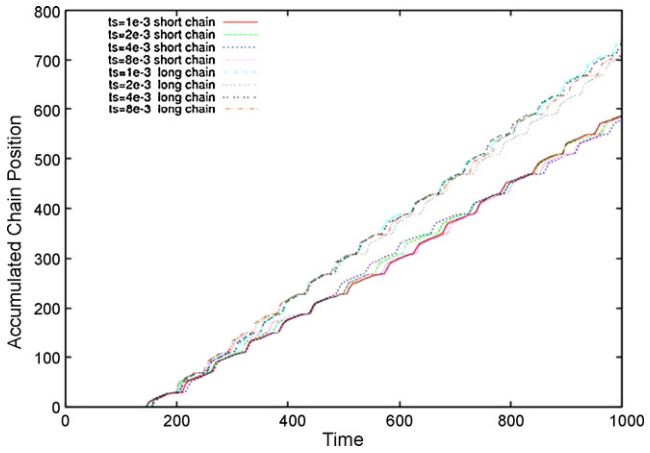

Fig. 6. Simulation results of molecules' horizontal movement using different time-steps.

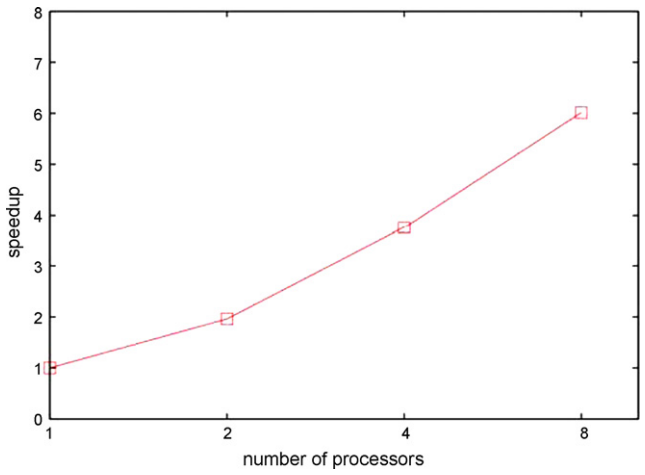

Fig. 7. Computational speedup with relation to number of processors.

time-steps are applied. Under different time-steps, there is little difference on the average velocity of the DNA. However, the velocity difference between short and long DNA are clearly present using all time-steps. It proves that our simulation captures the physics of DNA separation and the separation in our simulation is not an artifact. Separation occurs in all simulations regardless the time-step used.

Finally, we illustrate the performance of our parallel DPD code. The machine used is a Linux cluster consisting of nine computing nodes, where each node has two duo-core Intel Xeon processors. A Gigabit switch connects all the nodes. Fig. 7 shows the speedup using different number of processors. The code performs reasonably well for small number of processors.

9. Conclusions

In Han et al. [1,2], a novel nanometer channel device for the separation of long DNA molecules using an entropic trapping mechanism were fabricated. Alternating deep and shallow sections construct an array of traps where the DNA conformations must undergo coil-stretch changes in order to pass through the traps. They found that longer molecules moved faster than shorter ones. Han and Craighead [3] provided detailed theoretical analyses of this separation phenomena. In this paper, we studied this separation process through mesoscopic-scale numerical simulation. Specifically, the dissipative particle dynamics (DPD) method was employed due its capability of capturing the hydrodynamic interactions, which is a very important aspect in the separation process. We simulated the entire procedure of the DNA separation, including sample preparation and launch separation. We verified that the entropic trapping mechanism plays a vital role in Han et al.'s [1,2,3] nano-fluidic device. Through a parameter study, we confirm Han et al.'s [1,2,3] observation that a small voltage gives clear separation but long separation time, while a large voltage uses less time but produces less efficient separation. Our simulations also show that longer DNA strands do move faster than shorter ones, as observed in Han et al.'s [1,2] experiments. In addition, we also confirm that the delayed entrance is the cause of the entropic trapping. However, we found that corner trapping is not a contributor to the DNA separation process, as reported by Streek et al. [4].

References

[1] J. Han, S.W. Turner, H.G. Craighead, Entropic trapping and escape of long DNA molecules at submicron size constriction, Physical Review Letters 83 (8) (1999) 1688–1691.
[2] J. Han, H.G. Craighead, Separation of long DNA molecules in a microfabricated entropic trap array, Science 288 (2000) 1026–1029.
[3] J. Han, H.G. Craighead, Characterization and optimization of an entropic trap for DNA separation, Analytical Chemistry 74 (2002) 394–401.
[4] M. Streek, F. Schmid, T.T. Duong, A. Ros, Mechanisms of DNA separation in entropic trap arrays: a Brownian dynamics simulation, Journal of Biotechnology 112 (2004) 79–89.
[5] S.W.P. Turner, M. Cabodi, H.G. Craighead, Confinement-induced entropic recoil of sing DNA molecules in a nanofluidic structure, Physical Review Letters 88 (12) (2002) 128103.
[6] O. Bakajin, T.A.J. Duke, J. Tegenfeldt, C.F. Chou, S.S. Chan, R.H. Austin, E.C. Cox, Separation of 100-kilobase DNA molecules in 10 seconds, Analytical Chemistry 73 (24) (2001) 6053–6056.
[7] L.R. Huang, J.O. Tegenfeldt, J.J. Kraeft, J.C. Sturm, R.H. Austin, E.C. Cox, A DNA prism for high-speed continuous fractionation of large DNA molecules, Nature Biotechnology 20 (2002) 1048–1051.
[8] J. Fu, J. Yoo, J. Han, Molecular sieving in periodic free-energy landscape created by patterned nanofilter arrays, Physical Review Letters 97 (2006) 018103.
[9] J. Fu, R.B. Schoch, A.L. Stevens, S.R. Tannenbaum, J.Y. Han, A patterned anisotropic nanofluidic sieving structure for continuous-flow separation of DNA and proteins, Nature Nanotechnology 2 (2006) 121–128.
[10] F. Tessier, J. Labrie, G.W. Slater, Electrophoretic separation of long polyelectrolytes in submolecular-size constrains: a Monte Carlo Study, Macromolecules 25 (2002) 4791–4800.
[11] Lee, DNA dynamics in electrokinetically driven micro-/nano-converging flows. Ohio State University. Online document, 2007.
[12] T.T. Perkins, D.E. Smith, R.G. Larson, S. Chu, Stretching of a single tethered polymer in a uniform flow, Science 268 (5207) (1995) 83–87.
[13] J.L. Viovy, Electrophoresis of DNA and other polyelectrolytes: physical mechanisms, Review of Modern Physics 72 (3) (2000) 813–872.
[14] R.M. Jendrejack, J.J. de Pablo, M.D. Graham, Stochastic simulations of DNA in flow: dynamics and effects of hydrodynamic interactions, Journal of Chemical Physics 116 (17) (2002) 7752–7759.
[15] P.J. Hoogerbrugge, J.M.V.A. Koelman, Simulating microscopic hydrodynamic phenomena with dissipative particle dynamics, Europhysics Letters 19 (3) (1992) 155–160.
[16] P. Español, P.B. Warren, Statistical mechanics of dissipative particle dynamics, Europhysics Letter 30 (1995) 191.
[17] P. Español, Challenges in molecular simulations: dissipative particle dynamics revisited, ESF SIMU Programme Newsletter 4 (2002) 59–77.
[18] E.S. Boek, P.V. Coveney, H.N.W. Lekkerkerker, P. van der, Schoot, Simulating the rheology of dense colloidal suspensions using dissipative particle dynamics, Physical Review E 55 (3) (1997) 3124–3133.
[19] Y. Kong, C.W. Manke, W.G. Madden, Effect of solvent quality on the conformation and relaxation of polymers via dissipative particle dynamics, Journal of Chemical Physics 107 (2) (1997) 592–602.
[20] X. Fan, P.T. Nhan, S. Chen, X. Wu, T.Y. Ng, Simulating flow of DNA suspension using dissipative particle dynamics, Physics of Fluids 18 (2006) 063102.
[21] P.V. Coveney, K.E. Novik, Computer simulations of domain growth and phase separation in two-dimensional binary immiscible fluids using dissipative particle dynamics, Physical Review E 54 (5) (1996) 5134–5141.
[22] M. Liu, P. Meakin, H. Huang, Dissipative particle dynamics simulation of multiphase fluid flow in microchannels and microchannel networks, Physics of Fluids 19 (2007) 033302.
[23] P.T. UnderHill, P.S. Doyle, On the coarse-graining of polymers into bead-spring chains, Journal of Non-Newtonian Fluid Mechanics 122 (2004) 3–31.
[24] S.B. Smith, L. Finzi, C. Bustamante, Direct mechanical measurement of the elasticity of single DNA molecules by using magnetic beads, Science 258 (5085) (1992) 1122–1126.
[25] D.E. Smith, H.P. Babcock, S. Chu, Single-polymer dynamics in steady shear flow, Science 283 (5408) (1999) 1724–1727.
[26] C. Bustamante, Entropic elasticity of λ-phage DNA, Science 265 (1994) 1599–1600.
[27] J.F. Marko, E.D. Sigga, Stretching DNA, Macromolecules 28 (26) (1995) 8759–8770.
[28] J.M. Schurr, S.B. Smith, Theory for extension of a linear polyelectrolyte attached at one end in a electric field, Biopolymers 29 (1990) 1161–1165.
[29] V. Symeonidis, G.E. Karniadakis, B. Caswell, Dissipative particle dynamics simulations of polymer chains: scaling laws and shearing response compared to DNA experiments, Physical Review Letters 95 (2005) 076001.
[30] A.W. Lee, S.F. Edwards, The computer study of transport processes under extreme conditions, Journal of Physics C: Solid State Physics 5 (15) (1972) 1921–1929.
[31] M. Revenga, I. Zuniga, P. Espanol, Boundary models in DPD, International Journal of Modern Physics C 9 (8) (1998) 1319–1328.
[32] S.M. Willemsen, H.C.J. Hoefsloot, P.D. Iedema, No-slip boundary condition in dissipative particle dynamics, International Journal of Modern Physics C 11 (5) (2000) 881–890.
[33] M. Revenga, I. Zuniga, P. Espanol, Boundary conditions in dissipative particle dynamics, Computer Physics Communication 121–122 (1999) 309–311.
[34] D.H. Duc, P.T. Nhan, X. Fan, An implementation of no-slip boundary conditions in DPD, Computational Mechanics 35 (2004) 24–29.
[35] C.P. Lowe, An alternative approach to dissipative particle dynamics, Europhysics Letter 47 (2) (1999) 145–151.

[36] R.D. Groot, J.-P. Warren, Dissipative particle dynamics: bridging the gap between atomistic and mesoscopic simulation, Journal of Chemical Physics 107 (11) (1997) 4423–4435.
[37] A. Jakobesen, O. Mouritsen, G. Besold, Artifacts in dynamical simulations of coarse-grained model lipid bilayers, Journal of Chemical Physics 122 (2005) 204901.
[38] V. Symeonidis, G.E. Karniadakis, A family of time-staggered schemes for integrating hybrid DPD models for polymers: algorithms and applications, Journal of Computational Physics 218 (2006) 82–101.
[39] D.C. Rapaport, The Art of Molecular Dynamics Simulation, Cambridge University Press, Cambridge, 1995.
[40] P.G. de Gennes, Scaling Concepts in Polymer Physics, Cornell University Press, Ithaca, 1979.
[41] A.S. Panwar, S. Kumar, Time scales in polymer electrophoresis through narrow constrictions: a Brownian dynamics study, Macromolecules 39 (2006) 1279–1289.